Towards Water-jet Steerable Needles

Mahdieh Babaiasl[1], Fan Yang[2], and John P. Swensen[3]

***Abstract*— Water-jet technology has been used extensively for decades industrially for many applications including mining, plastic, metal, stone, wood, and produce cutting. The use of water-jet in medical applications has been developed more recently and it is used for different applications such as soft tissue resection, bone cutting, wound debridement, and surgery. In this paper, a new application of water-jet technology in the medical field is proposed, namely water-jet cutting at the tip of a needle with a long-term goal of steerable needles. A needle insertion system is designed and built, which has a custom-designed water-jet nozzle attached to a Nitinol needle as its "needle". Insertions with and without water-jet into 10%, 15% and 20% Poly (styrene-b-ethylene-co-butylene-b-styrene) triblock copolymer (SEBS) tissue-mimicking simulants are performed and the associated force data is measured using a force sensor at the base of the needle. The results of force *vs.* displacement show that the water-jet reduces the insertion force associated with traditional needles by eliminating tip forces. In this paper, a custom-designed straight nozzle is used to show the feasibility of water-jet steerable needles, whereas future work will focus on steerability using steerable nozzles. Depth of cut as a function of fluid velocity is also measured for different volumetric flow rates. The results show that depth of cut is a linear function of fluid velocity when the width of the water-jet nozzle is sufficiently small and smooth.**

I. INTRODUCTION

The use of high-pressure water in industry dates back over a century. In the mid-1880s, water-jets were first used in hydraulic mining to flush out coal from the working surface of a mine [1]. The development of high-pressure pumps makes the cutting of harder materials a possibility. To date, water-jet cutting has been used for cutting plastic, high-strength alloys, metals, stone, wood, and food products.

High-pressure water is generated by a pump and travels through a nozzle that accelerates it toward a target. A high-pressure pump is the heart of every water-jet system. There are two types of pumps that are mainly used in industrial applications: direct-drive pumps and intensifier pumps. These pumps are chosen based on the applications they are designed for. At the orifice, the potential energy of compressed water is transformed into high kinetic energy of water-jet.

Cutting occurs when energy is introduced into the material to overcome its chemical bindings in the structure of the material. For instance, thermal cutting methods use the energy of chemical reactions, electricity, or light to create high temperatures to melt or ablate the material at the point of cutting. Mechanical methods use the kinetic energy of the moving tool or create ductile materials by using pressure [1]. Water-jet cutting can be considered as a mechanical method in which energy of the high speed jet is applied to the work-piece. The water acts as a cooling agent also and leads to a very high quality cut–low kerf with low surface roughness.

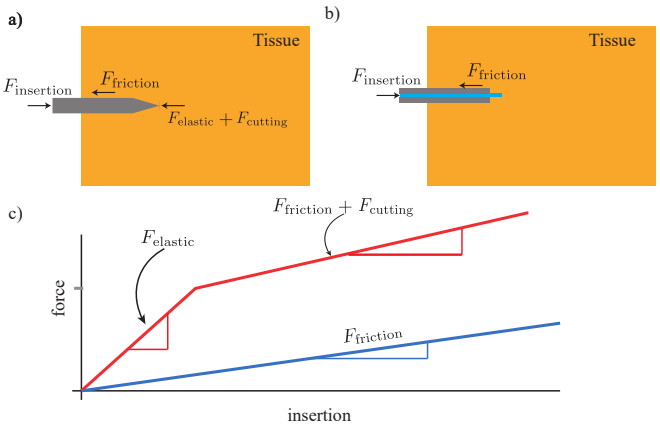

Fig. 1. Schematic of forces acting on the needle passing through the tissue for: (a) the no water-jet case with a traditional needle and (b) using water-jet cutting. $F_{elastic}$ is the elastic force that fractures the tissue and forms a crack (this force only exists before puncture and from the surface of the undeformed tissue to the maximally deformed one), $F_{cutting}$ is the cutting force and $F_{friction}$ is the friction force acting along the shaft of the needle (these two forces act on the needle from puncture to maximally inserting the needle and before exiting the tissue). (c) In the case of water-jet (blue schematic), the tip forces are eliminated, and only friction along the shaft of the needle exists (it is even expected to be lower than friction due to lubrication provided by water). For traditional needles (red schematic), insertion force can be defined as $F_{insertion} = F_{elastic} + F_{cutting} + F_{friction}$, and in the case of needle with water-jet, relationship $F_{insertion} = F_{friction}$ holds. Experimental results provided in section III also verified these relationships (Our results do not show $F_{elastic}$ because we started after puncture.)

Two types of water-jets have been used: (a) pure/ plain water jet (PWJ), where cutting is done by a high velocity water (high kinetic energy of water) and (b) abrasive water jet (AWJ), where plain water jet is generated in the orifice and flows through a mixing chamber that generates a vacuum pressure. In the case of AWJ, a dry solid abrasives is introduced into the chamber, commonly ruby particulates. Water, abrasives, and air are mixed and accelerated in the focusing tube. The role of the water in AWJ cutting is to accelerate the abrasive particles, flush out the debris from the cutting, and actively cool the workpiece [1].

Water-jet cutting has more recently been applied in medical applications. In surgery, PWJ is used to dissect organs, although this is not suitable for cutting bone because it

[1]Mahdieh Babaiasl is a graduate research assistant with the School of Mechanical and Materials Engineering, Washington State University, Pullman, Washington, USA. mahdieh.babaiasl@wsu.edu

[2]Fan Yang is a graduate research assistant with the School of Mechanical and Materials Engineering, Washington State University, Pullman, Washington, USA. fan.yang6@wsu.edu

[3]John P. Swensen is an assistant professor with the School of Mechanical and Materials Engineering, Washington State University, Pullman, Washington, USA. john.swensen@wsu.edu

requires pressures more than 75.84 MPa, which are not safe for surgery. AWJ can be a solution here since it can increase the cutting efficiency with less pressure. It should be noted that the abrasives used in AWJ cutting for surgery should be water-soluble and pharmacologically safe [2]. Water-jet techniques have also been used to resect liver [3], where a saline jet of 965.27 kPa was created using a standard agricultural electrically-driven spray system. Water-jets have also been used for dissections of liver [4], [5], [6], [7]. The efficiency of water jet for hepatic resections are examined in [8]. They came into conclusion that water jet dissection reduces large blood volume loss. The water jet system called the Helix Hydro-jet was introduced for dissection of Glioma and normal brain tissue. It has a hand-piece with nozzle of 100 μm in diameter [9]. In [10], the authors performed water-jet dissection of 50 porcine brains. They used different nozzle types $(80-150)$ μm and different levels of water-jet pressure $(96.57-3,999)$ kPa. They concluded that water-jet can dissect the brain parenchyma precisely with vessel preservation and that there is a linear relationship between water-jet pressure and depth of dissection. Water-jet is also used in renal surgery [11], [12]. They successfully removed the tumor of the lower pole of the left kidney and cleaned the renal parenchyma. Other medical applications of water-jet technology include wound debridement [13], orthopedic surgery [2], and bone cutting [14].

Water-jet cutting has several advantages compared to conventional cutting methods. One advantage of water-jet cutting is that because the water acts as a coolant, there are not temperature-related damages to the surrounding tissues, as seen with thermal ablation, grinding, or sawing. Second, water-jet cutting is precise, fast, and removes minimal material, where the water washes out the debris and leaves low-roughness surfaces. Using water-jet during surgery also decreases bleeding [8]. These advantages made water-jet to be appealing for medical applications.

Percutaneous therapies constitute a large fraction of medical procedures, including blood and tissue sampling, injecting drugs and anesthetics, implanting radioactive seeds, *etc.* In brachytherapy cancer treatment and tissue biopsy, needles are used to reach precise locations in the body. High insertion forces can complicate reaching the intended target with high accuracy. Research shows that lower insertion force can reduce needle bending and tissue deflection [15]. It can also reduce the pain felt by the patient during the procedure [16]. Therefore, researchers have actively researched ways to reduce the insertion forces. Methods proposed in the literature to reduce the insertion forces include changing needle geometry [17], [18], using smaller needles [19], and inserting the needle with different insertion speeds and/or vibration [20].

Measuring insertion forces and needle tissue-interaction forces for traditional needles are previously introduced in the literature [21], [22], [23], however, to the best of our knowledge, this is the first time that water-jet is incorporated into traditional needles and insertion forces are measured.

Figure 1 depicts forces acting on the needle in traditional needle insertion and in the proposed water-jet method. $F_{elastic}$ is the elastic force that fractures the tissue and forms a crack. This force exists before puncturing the tissue and acts on the needle from point at which the needle comes in contact with the undeformed surface of the tissue to when tissue is maximally deformed, just prior to puncture. Our experimental results do not show this force because we started to collect data after puncture. $F_{cutting}$ is the cutting force, and $F_{friction}$ is the friction force acting along the shaft of the needle. The red line depicts the forces acting on the needle in the case of traditional needles, and the blue diagram is the force acting on the needle in the case of water-jet needle, which is only friction. Our experimental results showed that the frictional force with the waterjet is even lower than a traditional needle, likely due to lubrication provided by the water during insertion.

In this paper, a new system for water-jet needles is proposed. To the best of the authors' knowledge, this is the first time that water-jet is used in percutaneous applications, and the authors found no prior studies on waterjet steerable needles. It is shown that using water-jet, the tip forces are eliminated and only the friction force remains. To explain it more precisely, the insertion force experienced by a physician (or robot) at the base of the needle has been reduced. This force experienced at the base of the needle is the combination of elastic, friction, and cutting force at the tip.The proposed method reduces the forces that build up at the tip and are transmitted along the shaft of the needle back to the user at the base of the needle. Much of that force that is experienced by the user at the base of the needle is due to the elastic buildup at the tip that is necessary to cause sufficient pressure at the very tip of the needle to start fracture. With the water jet, this elastic buildup is not necessary because the 300μm waterjet is only putting pressure on the tiny amount of tissue it is trying to fracture. The second reason is looking forward to needles that are curving in tissue that experience buckling, and using waterjet, this effect will be eliminated. The depth of water-jet cut as a function of fluid velocity is also measured. It is found that there is a linear relationship between depth of cut and fluid velocity when the width of the water-jet nozzle is sufficiently small and smooth. The experiments presented in this paper are focused on demonstrating the potential of water-jet directed needles, and work is currently underway to develop sub-millimeter, controllable nozzles at the tip of the needle with the purpose of steerable needles, hence this is a substantive step towards waterjet-directed steerable needles.

II. MATERIALS AND METHODS

A. Tissue Preparation

Common materials for tissue-mimicking simulants are gelatin, rubbers, leather, silicon elastomers, soap, lard and clay [24]. These materials can provide an average representation of the soft tissue. In the case of gelatin, the ratio of solid content to water can be changed to alter the mechanical properties. Most common combinations of gelatin are 10% and 20% solid with the remaining water. The amount of

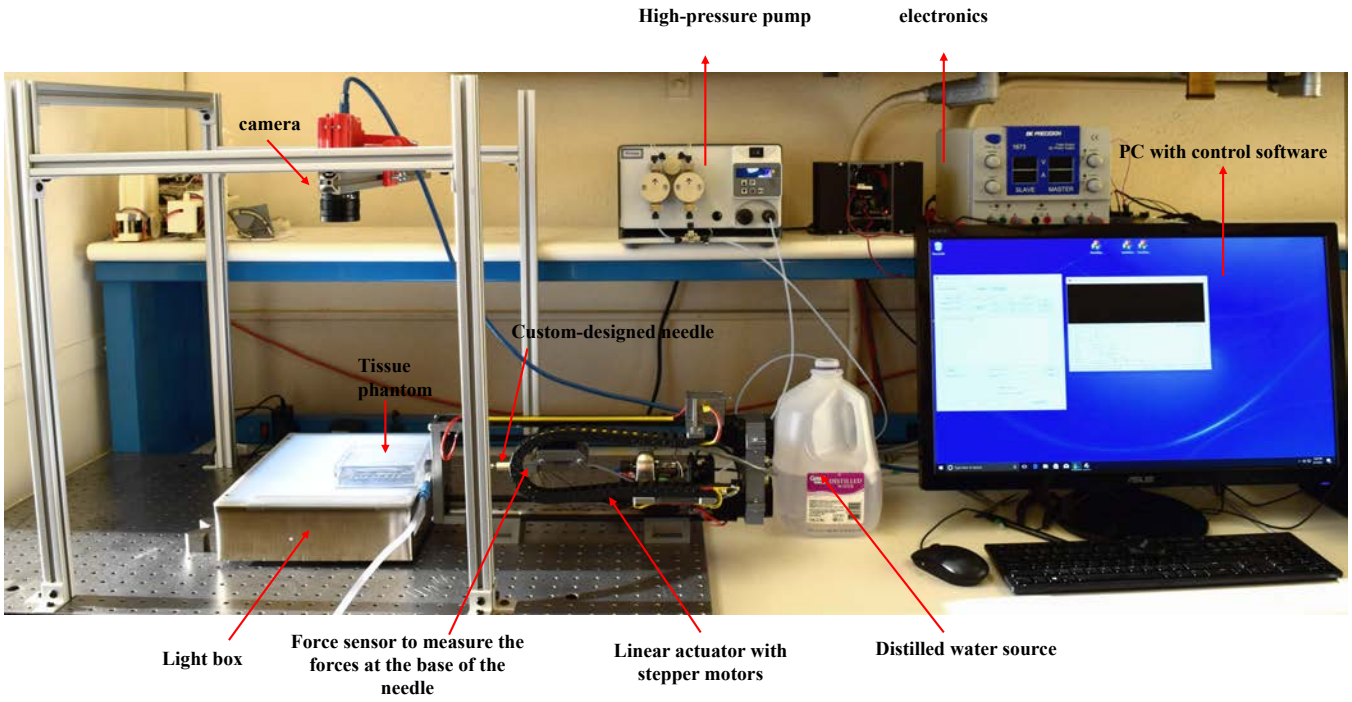

Fig. 2. Experimental setup of the water-jet system. A linear actuator drives the needle into tissue with a given velocity of insertion adjusted in the customized software. A high-pressure pump with changeable flow rate is used to create high-pressure water for experiments with water-jet. A load cell at the base of the needle measures insertion forces and the data are gathered in the control software.

solid determines the softness of the gel. Water-based nature of gelatin causes time, temperature and humidity-dependent issues. Properties can be changed due to excessive heating during production or storage. The advantage of using SEBS as the tissue simulant material is containing non-aqueous solvents, which makes it more environmentally stable substitute for water-based hydrogels (such as gelatin) in terms of increased operational temperature ranges, and lifetimes. Additionally, SEBS tissues are optically clear, their Young's modulus can easily be altered by changing the polymer content, they have low Young's modulus but high fracture toughness, which is similar to bio-tissues, and lower friction than many other materials with low Young's modulus like silicone rubbers.

Poly (styrene-b-ethylene-co-butylene-b-styrene) triblock copolymer (SEBS), Kraton Polymers LLC (G1652, Houston, TX, USA) is used as the main ingredient of tissue-mimicking phantom. Light mineral oil is used as the solvent. SEBS material and mineral oil are weighed out to produce mixtures containing 10, 15 and 20 vol% SEBS. The mixture was then put into the oven at 120^o C for 6 hours (for mixtures containing a lower amount of SEBS this time is lower) and was mixed occasionally to produce a homogeneous solution without any visible undissolved powder. It was degassed afterwards using a vacuum chamber to eliminate any air bubble trapped in the solution. The solution is then poured into rectangular molds of dimensions $100 \times 100 \times 50$ mm, then let to cool down in room temperature before removing from the molds. The Young's modulus of these tissue simulants can be found from (1), which we derived from the log-log plot of the Young's modulus versus polymer fraction figure presented in [25].

$$Young's\ modulus = c(Polymer\ fraction)^m \qquad (1)$$

Where $c = 4.6018 \times 10^6$ and $m = 2.2234$. Therefore, the Young's modulus of 10%, 15% and 20% SEBS are 27, 68, and 128 kPa, respectively, which are relevant to stiffnesses of real biological tissues [26]. In particular, Young's moduli of 10%, 15%, and 20% are similar to uterus, and cervix tissues, the Young's moduli of which are in the range of $30-90$ kPa [27], prostate in the range of $62-69$ kPa [28], thrombus in the range of $8-38$ kPa [29], breast with modulus of 29 kPa [30], and muscle in the range of $7-57$ kPa [31], [32].

B. Experimental Setup

The experimental setup used for all experiments is shown in Fig. 2. A linear actuator is used to drive the needle into the tissue simulant with velocity of insertions 1, 5, and 10 $\frac{mm}{s}$. These insertion velocities are known to be relevant to insertions in real medical applications [33]. These velocities can be adjusted in the designed graphical user interface (GUI) by setting the depth of insertion and time. This multi-threaded application developed using Microsoft Visual C++ is not only capable of communicating with and controlling the needle experiment but also reading the force sensor and control the pump system through serial communications.

This user interface records data to a .CSV file and is capable of feedback control.

To allow high-fidelity control of volumetric flow rate and the ability to measure pressure at the pump, an off-the-shelf pump traditionally used for high-performance liquid chromatography (HPLC) named PR-class Dual Piston is used (PR100PFT3D, Scientific Systems Inc., State College, PA, USA). This system can provide pressures up to 27.58 MPa and flow rates up to 100 $\frac{mL}{min}$ at the maximum pressure. Pure distilled water used in this PWJ cutting system and a suction system attached near the base of the needle avoids the water from splashing while inserting and cutting. Fig. 3 shows the custom-designed suction system. One major concern here may be the volume of the water that needs to be cleared from the cutting area. It seems that if the water is not cleared fast enough, the remaining pressure near the needle tip causes potential problems with the surrounding tissue and diminish the effectiveness of the water cutting. However, the reality is that in waterjet insertions while the water hits and cuts the tissue the majority of it splashes back and is gathered in a box that is attached to a strong suction system that does not let water to be trapped in the cutting path.

Fig. 3. Custom-designed suction system. It includes a 3D printed part near the base of the needle that collects the water sprayed back while running water-jet experiments. The collected water is then sucked by a suction canister attached to a vacuum pump.

For the water-jet nozzle, first, a piece of 1.59 mm copper tubing is cut to about 45 mm of length. Then, a piece of Nitinol is cut and sanded to remove the oxide layer, so that the solder would adhere. Next, the Nitinol wire was soldered inside the 1.59 mm copper tubing. Finally, the copper tubing is attached to the ferruled reducer, and then to the water pump via standard tubing. The Nitinol tube acts as a needle with inner diameter of 0.32 mm, and outer diameter of 0.58 mm. Superelastic properties of Nitinol makes it a good candidate to be used as a material for steerable needles [34]. Fig. 4 represents the custom-designed needle used in needle insertions with and without water-jet.

While the force sensor records the insertion forces, a high-resolution camera is used to take pictures during insertion or cutting experiments to measure the depth of cut as a function of fluid velocity.

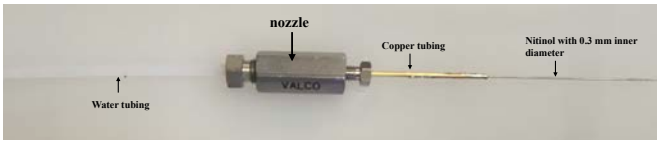

Fig. 4. Custom-designed needle for insertions. The needle consists of a copper tubing soldered to a superelastic material named Nitinol as its "needle". The copper tubing is attached to a ferruled reducer, and then standard tubing.

C. Force measurement using insertions with and without water-jet

Three distinct experiments are conducted to compare the insertion forces of traditional needles and waterjet needles. These include: (a) insertion of a needle without the waterjet to give a baseline for a traditional needle's insertion forces, (b) reinserting a needle without waterjet in the existing channel from (a) to determine the frictional component of (a), and (c) a new insertion with the waterjet enabled (in a fresh channel) to compare the insertion forces against both the traditional needle insertion and the friction-only component of a traditional insertion.

These three different tests are done on 10%, 15% and 20% SEBS tissues, with each test sample of size $100 \times 100 \times 50$ mm. First, the needle is inserted into the tissue with velocities of insertion of 1, 5, and 10 $\frac{mm}{s}$ using the linear actuator and without running the water-jet. These insertion velocities are relevant to insertion velocities during clinical percutaneous needle insertion procedures [33]. The needle is inserted 50 mm through the tissue and force data is recorded at the rate of 5 data per second using the customized GUI. The data is recorded until the needle reaches the maximum insertion depth. The needle is then retracted and reinserted into the same channel using the same velocity of insertion and without water running and the force data for the second insertion in the same channel is also recorded. This second insertion in the same channel is intended to disambiguate the frictional forces from the cutting forces at the tip for the non-waterjet scenario. To insure that the needle will follow the same path, the setup was remained unchanged between the two sets of experiments. Then, another insertion is conducted when the pump is turned on with volumetric flow rates of 10, 20, and 30 $\frac{mL}{min}$ for 10%, 15%, and 20% SEBS tissues, respectively. In these trials, the needle is inserted with same velocities of insertion along with the jet of water that cuts a small distance in front of the needle to let the needle pass the tissue. 10 experiments are done for each stage, with total of 90 experiments for each tissue so 3 (tissues) $\times$ 3 (velocities of insertion) $\times$ 3 (number of different tests) $\times$ 10 (number of experiments in each stage) $=$ 270 experiments are done and the average of 10 experiments and the standard deviation of data are calculated for each stage, so that the results are statistically meaningful.

D. Measuring depth of cut of water-jet as a function of fluid velocity

The needle is inserted about 2 cm into the $100 \times 100 \times 50$ mm SEBS tissue. Using a high-resolution camera mounted above the tissue and using a light-box underneath the tissue, a photo is captured before the waterjet is enabled. The pump is then turned on with a specific volumetric flow rate and after $30(s)$, the pump was turned off and another photo was taken showing the depth of cut of the water-jet in front of the needle. For better visibility, edible food colors are added to water. The volumetric flow rate is varied between 20 and 80 $\frac{mL}{min}$. For each flow rate, 5 experiments are conducted and the photos are processed using a customized Matlab program that measures the depth of cut in front of the needle from the pixels of the photo based on the calibrated measurement provided by the ruler on the light-box. Fig. 5 depicts an example of the output of this software. Fig. 7 shows an example of before and after photos of depth of cut measurements.

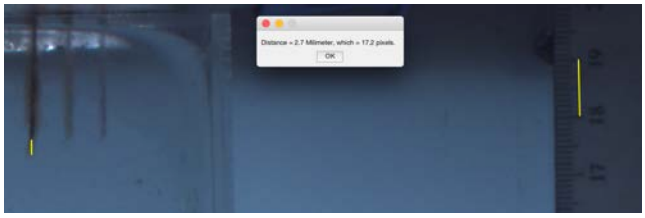

Fig. 5. The output of the developed software in Matlab to measure the depth of cut. The software first loads the image and zooms in the area of interest. Then it asks to select a real world measurement and enter the real value of it (10 mm in the example) for calibration. Then the user will select the area of interest to measure, and the software associates the pixel distance to a real-world measurement.

III. Results, and Discussion

In this section, results of tests with insertions with and without water-jet are provided. In the first subsection, results of force measurements with and without water-jet are presented and demonstrate how using the water-jet for cutting can decrease the insertion force by eliminating tip forces. In the second subsection, results of depth of cut as a function of fluid velocity are given and shown that there is a linear relationship between depth of cut and fluid velocity when the width of the water-jet nozzle is sufficiently small and smooth.

A. Waterjet Needles Result in a Reduction in Insertion Force of Over 50 %

The average force from 3 different experiments on each tissue is plotted against the needle displacement. Fig. 6 shows the force *vs.* displacement for insertions with no water, no water reinsertion through the same channel, and with water-jet for 10%, 15% and 20% SEBS tissues with 3 different velocities of insertion. The bars on the figure represent one standard deviation above and one standard deviation below the data. The following results can be observed from these figures:

- Comparing the forces in the case of insertions with no water and insertions with water-jet, it is apparent that water-jet reduces the insertion force by eliminating the tip forces and only friction force exists. The total insertion force by water jet is even lower, and the authors propose that this is due to the lubrication effect of the water in the channel.
- The needle passing through the tissue (in traditional needle insertion methods) experiences different phases of cutting. In phase 1, the tissue deflects and the force gradually rises due to elastic forces. This occurs from the surface of the undeformed tissue to when the tissue is maximally deformed (before puncture). This is represented in Fig. 1 as $F_{elastic}$. The results shown in Fig. 6 do not include this stage since we started to gather the data after puncture. In phase 2, the tissue is cut and initial crack is formed (puncture). Needle geometry widens the crack and the needle passes through with friction acting between the needle and the tissue. This is from when puncture occurs till the needle is inserted maximally into the tissue. This is expressed as $F_{cutting} + F_{friction}$ in the top panel of Fig. 1 - c. This stage is obvious in our results with traditional needle insertion. There is also phase 3 that the needle exits the tissue and only the frictional force is present. This stage is not relevant to our data since we went 50 mm into the tissue and did not pass all the way through it. These 3 stages are consistent with previous research on traditional needle insertions [35].
- The 20% SEBS tissue has a higher frictional force. This is in agreement with standard sliding friction models where the friction is a function of a coefficient and the normal force (or normal pressure across the surface area). In the case of the 20%, even though the needle is the same size and displacing the same amount of tissue, because it has a higher elastic modulus then the normal force/pressure will be higher for the same volume of tissue displaced by the needle.
- The insertion forces in both the traditional needle insertions and in water-jet needle insertions show a rate-dependent behavior. The forces are higher for higher velocities of insertions. This observation is consistent with previous research in needle insertions [36].
- The frictional force is dependent on the depth of insertion, and increases as the insertion depth increases. It also depends on the stiffness of the tissue. These observations are in line with previous research on traditional needle insertions [21]. This will lead to overall increased insertion force in stiffer tissues.
- The purpose of using needles in the first place is to reduce the tear in the tissue while accessing a target. It may seem that waterjet increases tear surrounding the needle, but considering that the diameter of water jet is smaller than the needle and the time that the water jet is in contact with the tissue is so small, only a small cutting in front of the needle will be achieved and there is not enough time for the water-jet to tear the

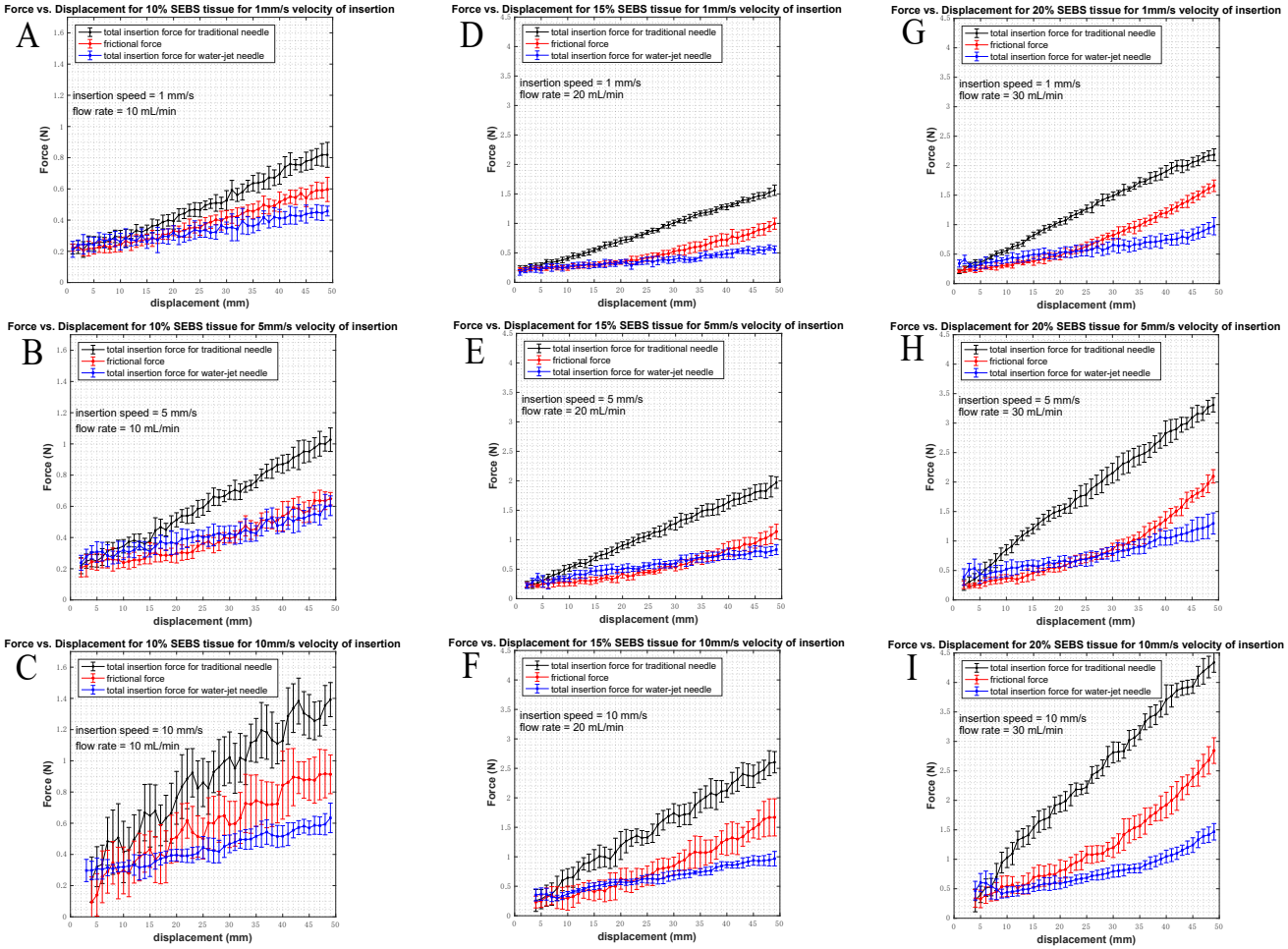

Fig. 6. Force *vs.* displacement measurement for ten trials each in: (A - C) 10% SEBS tissue simulant with 3 different velocities of insertion (D - F) 15% SEBS tissue simulant with 3 different velocities of insertion, and (G - I) 20% SEBS tissue simulant with 3 different velocities of insertion. The black plot (the one with circles) shows the total insertion force in the case of traditional needle insertion after puncture. This force is equal to $F_{cutting} + F_{friction}$. The red plot (the one with asterisks) depicts only friction force ($F_{friction}$) (acquired with inserting the needle into the previously cut channel). The last plot (blue one with squares) represents the total insertion force with water-jet needle. As is evident from all figures, total insertion force using water-jet is even lower than the friction force since water-jet eliminates tip forces and lubricates the channel while insertion.

surrounding tissue. This can be achieved by calculating an optimum velocity of insertion that ensures small cutting and avoids the tear and damage to the tissue.

B. The Depth of Cut is a Linear Function of the Fluid Velocity

Fig. 8 depicts the average measurements of depth of cut as a function of fluid velocity for 15% (up) and 20% (down) SEBS tissues. A line is fitted to experimental data and as can be seen the goodness of the fit, which is quantified by the coefficient of determination is 0.9884 for the 15% SEBS tissue, and 0.9181 for the 20% SEBS tissue. This gives a linear relationship between the depth of cut and the flow rate when the width of the water-jet nozzle is sufficiently small and smooth and is expressed by (2), which can be used to predict the depth of cut (DOC) for higher flow rates. It is also observed that there is a minimum flow rate that the cutting occurs and it is higher for the stiffer tissue. On the other hand, for higher flow rates, it is observed that the water also cuts more of the surrounding tissue which is undesirable. For needle steering purposes, usually larger depth of cut is not necessary and it is important that a small amount is cut and then the needle follows the path.

$$DOC = c_1(FR) + c_2 \tag{2}$$

In this equation, $c_1 = 0.1439$, and $c_2 = -2.653$ for 15% SEBS and $c_1 = 0.08134$, and $c_2 = -1.553$ for 20% SEBS.

It should be noted here that depth measurement analysis was done using homogeneous phantoms, SEBS tissue simulants. The created fits for cutting depth measurements would work fine with the same type of phantom, but whether these results can be generalized to be used in other heterogeneous phantoms, and also for in vivo is still under research by our group.

IV. CONCLUSIONS AND FUTURE WORK

In this paper, a new system was proposed for water-jet needles insertion. While the data presented in this paper only

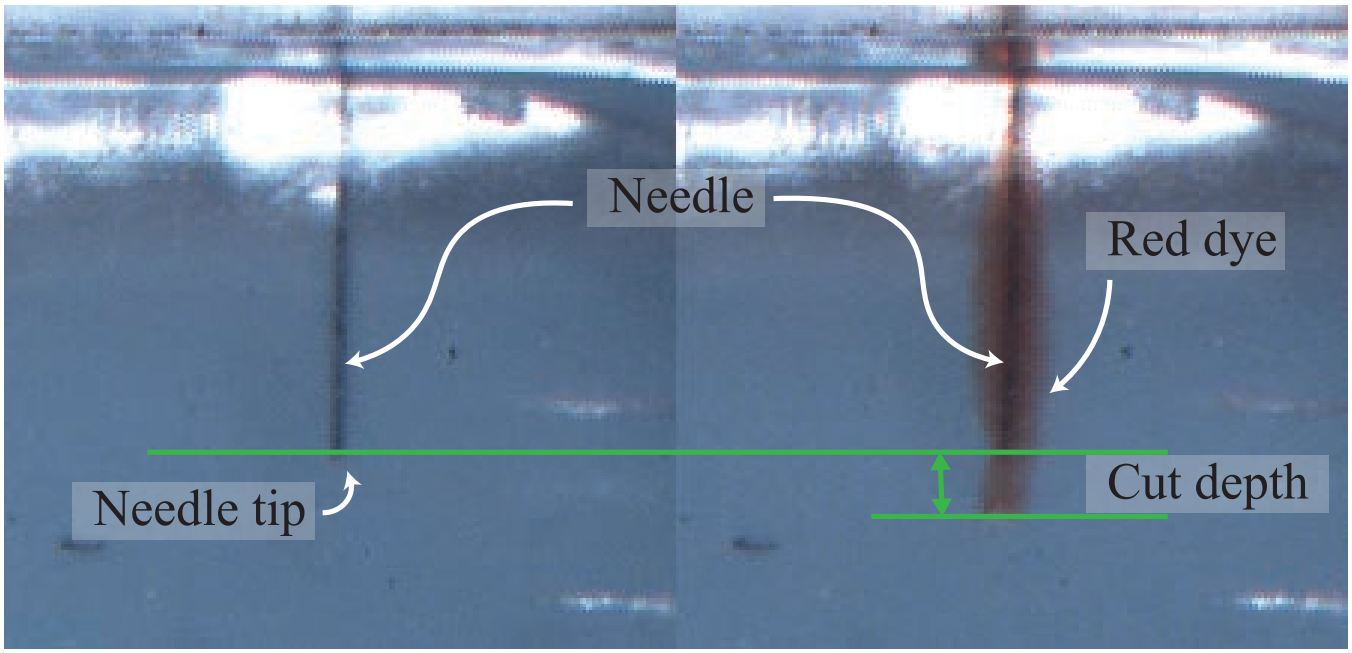

Fig. 7. An example of before and after photos of measuring depth of cut. The needle is initially inserted into tissue about 2 cm and then the pump is running with a given flow rate, say 60 $\frac{mL}{min}$ (only in this example) for 30 (s). Then, the pump is turned off and another photo is taken. This photo is imported into a customized program in MatLab that changes the measured pixels of depth of cut to mm through a calibration using the provided ruler on the light-box. For better visibility, food color is added to water.

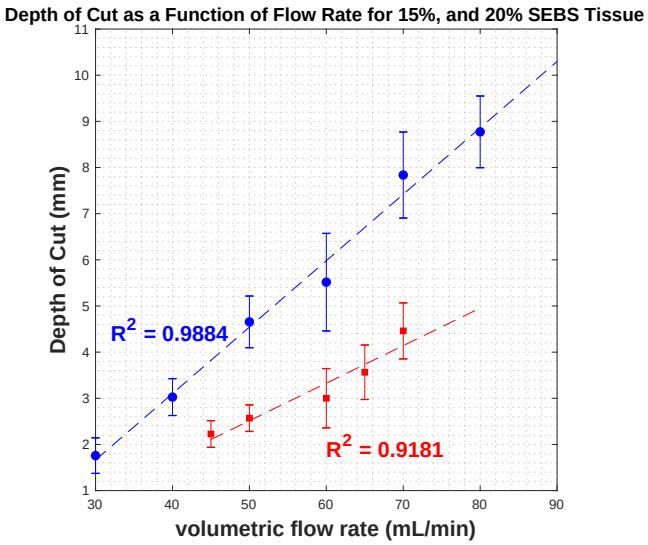

Fig. 8. Depth of cut as a function of fluid velocity for 15% (blue circles and fitted line) and 20% (red squares and fitted line) SEBS tissue. As can be seen there is a linear relationship between depth of cut and fluid velocity when the width of the water-jet nozzle is sufficiently small and smooth. 5 experiments are conducted for each flow rate and the average of them are reported in this figure. The bars on the graph show one standard deviation above and below the mean. Circles and squares show the experimental data, and the dotted lines show the lines fitted to experimental data.

presents straight trajectory insertions, this work is intended as a proof of feasibility in using water-jet at the tip of a needle to accurately control the tissue fracture. Future work currently underway involves the development of sub-millimeter controllable nozzles such that the direction of tissue fracture can also be controlled, thus providing steerable needle using the same method. Even in the absence of a steerable tip, the proposed method can allow for accurate straight-trajectory insertions, even across tissue changes and membrane boundaries, where such trajectories are desirable.

A linear actuator was utilized to drive the needle into tissue with known insertion velocity. Force data were collected in the experiments with and without water-jet. The results with the force data showed that this method can be used as a promising method to decrease the insertion force, which is very important in medical applications. Depth of cut was measured as a function of flow rate and it was shown that it is a linear function of the flow rate when the width of the water-jet nozzle is sufficiently small and smooth.

Future work also involves finding a physics-based model to predict cutting depth and insertion force based on parameters such as tissue toughness, tissue stiffness, nozzle diameter, volumetric flow rate of the cutting tissue, density adjustment of saline, and transitioning to experiments with real biological tissues.

ACKNOWLEDGMENT

The authors would like to thank Alex Rodriguez, and Sean Journot for their help on preparing the experimental setup.

REFERENCES

[1] D. A. Summers, *Waterjetting technology*. CRC Press, 2003.

[2] K. Schwieger, V. Carrero, R. Rentzsch, A. Becker, N. Bishop, E. Hille, H. Louis, M. Morlock, and M. Honl, "Abrasive water jet cutting as a new procedure for cutting cancellous bonein vitro testing in comparison with the oscillating saw," *Journal of Biomedical Materials Research Part B: Applied Biomaterials*, vol. 71, no. 2, pp. 223–228, 2004.

[3] D. N. Papachristou and R. Barters, "Resection of the liver with a water jet," *British journal of Surgery*, vol. 69, no. 2, pp. 93–94, 1982.

[4] B. Persson, B. Jeppsson, K. Tranberg, K. Roslund, and S. Bengmark, "Transection of the liver with a water jet," *Surg Gynecol Obstet*, vol. 168, no. 3, pp. 267–268, 1989.

[5] Y. Une, J. Uchino, T. Horie, Y. Sato, K. Ogasawara, A. Kakita, and F. Sano, "Liver resection using a water jet," *Cancer chemotherapy and pharmacology*, vol. 23, pp. S74–S77, 1989.

[6] H. Baer, G. Maddern, and L. Blumgart, "Hepatic surgery facilitated by a new jet dissector," *HPB Surgery*, vol. 4, no. 2, pp. 137–146, 1991.

[7] ——, "New water-jet dissector: initial experience in hepatic surgery." *The British journal of surgery*, vol. 78, no. 4, p. 502, 1991.

[8] C. M. Vollmer, E. Dixon, A. Sahajpal, M. S. Cattral, D. R. Grant, S. Gallinger, B. R. Taylor, and P. D. Greig, "Water-jet dissection for parenchymal division during hepatectomy," *HPB*, vol. 8, no. 5, pp. 377–385, 2006.

[9] J. Piek, J. Oertel, and M. Robert Gaab, "Waterjet dissection in neurosurgical procedures: clinical results in 35 patients," *Journal of neurosurgery*, vol. 96, no. 4, pp. 690–696, 2002.

[10] J. Oertel, M. R. Gaab, A. Knapp, H. Essig, R. Warzok, and J. Piek, "Water jet dissection in neurosurgery: experimental results in the porcine cadaveric brain," *Neurosurgery*, vol. 52, no. 1, pp. 153–159, 2003.

[11] J. Hubert, E. Mourey, J. Suty, A. Coissard, J. Floquet, and P. Mangin, "Water-jet dissection in renal surgery: experimental study of a new device in the pig," *Urological research*, vol. 24, no. 6, pp. 355–359, 1996.

[12] R. D. Penchev, J. E. Losanoff, and K. T. Kjossev, "Reconstructive renal surgery using a water jet," *The Journal of urology*, vol. 162, no. 3, pp. 772–774, 1999.

[13] R. Gurunluoglu, "Experiences with waterjet hydrosurgery system in wound debridement," *World Journal of Emergency Surgery*, vol. 2, no. 1, p. 10, 2007.

[14] S. Hloch, J. Valicek, and D. Kozak, "Preliminary results of experimental cutting of porcine bones by abrasive waterjet," *Tehnicki Vjesnik-Technical Gazette*, vol. 18, no. 3, pp. 467–470, 2011.

[15] Y. R. van Veen, A. Jahya, and S. Misra, "Macroscopic and microscopic observations of needle insertion into gels," *Proceedings of the Institution of Mechanical Engineers, Part H: Journal of Engineering in Medicine*, vol. 226, no. 6, pp. 441–449, 2012.

[16] H. Egekvist, P. Bjerring, and L. Arendt-Nielsen, "Pain and mechanical injury of human skin following needle insertions," *European journal of pain*, vol. 3, no. 1, pp. 41–49, 1999.

[17] T. Podder, D. Clark, J. Sherman, D. Fuller, E. Messing, D. Rubens, J. Strang, Y. Zhang, W. ODell, W. Ng, *et al.*, "Effects of tip geometry of surgical needles: an assessment of force and deflection," in *IFMBE Proc*, vol. 11, no. 1, 2005, pp. 1727–1983.

[18] Y. Wang, B. L. Tai, R. K. Chen, and A. J. Shih, "The needle with lancet point: geometry for needle tip grinding and tissue insertion force," *Journal of Manufacturing Science and Engineering*, vol. 135, no. 4, p. 041010, 2013.

[19] S. P. Davis, B. J. Landis, Z. H. Adams, M. G. Allen, and M. R. Prausnitz, "Insertion of microneedles into skin: measurement and prediction of insertion force and needle fracture force," *Journal of biomechanics*, vol. 37, no. 8, pp. 1155–1163, 2004.

[20] M. Heverly, P. Dupont, and J. Triedman, "Trajectory optimization for dynamic needle insertion," in *Robotics and Automation, 2005. ICRA 2005. Proceedings of the 2005 IEEE International Conference on*. IEEE, 2005, pp. 1646–1651.

[21] R. J. Roesthuis, Y. R. Van Veen, A. Jahya, and S. Misra, "Mechanics of needle-tissue interaction," in *Intelligent Robots and Systems (IROS), 2011 IEEE/RSJ International Conference on*. IEEE, 2011, pp. 2557–2563.

[22] M. Mahvash and P. E. Dupont, "Mechanics of dynamic needle insertion into a biological material," *IEEE Transactions on Biomedical Engineering*, vol. 57, no. 4, pp. 934–943, 2010.

[23] S. Misra, K. B. Reed, B. W. Schafer, K. Ramesh, and A. M. Okamura, "Mechanics of flexible needles robotically steered through soft tissue," *The International journal of robotics research*, vol. 29, no. 13, pp. 1640–1660, 2010.

[24] G. Appleby-Thomas, P. Hazell, J. Wilgeroth, C. Shepherd, D. Wood, and A. Roberts, "On the dynamic behavior of three readily available soft tissue simulants," *Journal of Applied Physics*, vol. 109, no. 8, p. 084701, 2011.

[25] R. A. Mrozek, B. Leighliter, C. S. Gold, I. R. Beringer, H. Y. Jian, M. R. VanLandingham, P. Moy, M. H. Foster, and J. L. Lenhart, "The relationship between mechanical properties and ballistic penetration depth in a viscoelastic gel," *Journal of the mechanical behavior of biomedical materials*, vol. 44, pp. 109–120, 2015.

[26] P. N. Wells and H.-D. Liang, "Medical ultrasound: imaging of soft tissue strain and elasticity," *Journal of the Royal Society Interface*, vol. 8, no. 64, pp. 1521–1549, 2011.

[27] M. Z. Kiss, M. A. Hobson, T. Varghese, J. Harter, M. A. Kliewer, E. M. Hartenbach, and J. A. Zagzebski, "Frequency-dependent complex modulus of the uterus: preliminary results," *Physics in Medicine & Biology*, vol. 51, no. 15, p. 3683, 2006.

[28] T. A. Krouskop, T. M. Wheeler, F. Kallel, B. S. Garra, and T. Hall, "Elastic moduli of breast and prostate tissues under compression," *Ultrasonic imaging*, vol. 20, no. 4, pp. 260–274, 1998.

[29] H. Xie, K. Kim, S. R. Aglyamov, S. Y. Emelianov, M. ODonnell, W. F. Weitzel, S. K. Wrobleski, D. D. Myers, T. W. Wakefield, and J. M. Rubin, "Correspondence of ultrasound elasticity imaging to direct mechanical measurement in aging dvt in rats," *Ultrasound in Medicine and Biology*, vol. 31, no. 10, pp. 1351–1359, 2005.

[30] L. Han, J. A. Noble, and M. Burcher, "A novel ultrasound indentation system for measuring biomechanical properties of in vivo soft tissue," *Ultrasound in Medicine and Biology*, vol. 29, no. 6, pp. 813–823, 2003.

[31] K. Parker, S. Huang, R. Musulin, and R. Lerner, "Tissue response to mechanical vibrations for sonoelasticity imaging," *Ultrasound in Medicine and Biology*, vol. 16, no. 3, pp. 241–246, 1990.

[32] S. F. Levinson, M. Shinagawa, and T. Sato, "Sonoelastic determination of human skeletal muscle elasticity," *Journal of biomechanics*, vol. 28, no. 10, pp. 1145–1154, 1995.

[33] N. Abolhassani, R. Patel, and M. Moallem, "Control of soft tissue deformation during robotic needle insertion," *Minimally invasive therapy & allied technologies*, vol. 15, no. 3, pp. 165–176, 2006.

[34] T. Duerig, A. Pelton, and D. Stöckel, "An overview of nitinol medical applications," *Materials Science and Engineering: A*, vol. 273, pp. 149–160, 1999.

[35] S. Jiang, P. Li, Y. Yu, J. Liu, and Z. Yang, "Experimental study of needle–tissue interaction forces: effect of needle geometries, insertion methods and tissue characteristics," *Journal of biomechanics*, vol. 47, no. 13, pp. 3344–3353, 2014.

[36] J. R. Crouch, C. M. Schneider, J. Wainer, and A. M. Okamura, "A velocity-dependent model for needle insertion in soft tissue," in *International Conference on Medical Image Computing and Computer-Assisted Intervention*. Springer, 2005, pp. 624–632.